Article

Tuning Intrinsic and Extrinsic Proton Conduction in Metal-Organic Frameworks by the Lanthanide Contraction

Norman E. Wong, Padmini Ramaswamy, Andrew Lee, Benjamin S. Gelfand, Kamila Bladek, Jared M. Taylor, Denis Spasyuk, and George K. H. Shimizu

J. Am. Chem. Soc., **Just Accepted Manuscript** • DOI: 10.1021/jacs.7b07987 • Publication Date (Web): 27 Sep 2017

Tuning Intrinsic and Extrinsic Proton Conduction in Metal-Organic Frameworks by the Lanthanide Contraction

Norman E. Wong,[a] Padmini Ramaswamy,[a] Andrew S. Lee,[a] Benjamin S. Gelfand,[a] Kamila J. Bladek,[a] Jared M. Taylor[a], Denis M. Spasyuk[b] and George K. H. Shimizu[a]*

a Department of Chemistry, University of Calgary. 2500 University Dr. NW Calgary, Alberta, Canada, T2N 1N4.

b Canadian Macromolecular Crystallography Facility, Canadian Light Source Inc. 44 Innovation Boulevard, Saskatoon, Saskatchewan, Canada. S7N 2V3.

KEYWORDS: Proton conduction, metal-organic framework, lanthanide, phosphonate, grain boundary

ABSTRACT: Seven isomorphous lanthanide metal-organic frameworks in the PCMOF-5 family, [Ln(H5L)(H2O)n](H2O) (L = 1,2,4,5-tetrakis(phosphonomethyl)benzene, Ln= La, Ce, Pr, Nd, Sm, Eu, Gd) have been synthesized and characterized. This family contains 1-D water-filled channels lined with free hydrogen phosphonate groups and gives a very low activation energy pathway for proton transfer. The lanthanide contraction was employed to systematically vary the unit cell dimensions and tune the proton conducting pathways. LeBail fitting of the crystalline series shows that the crystallographic *a* axis, along the channel, can be varied in increments less than 0.02 Å correspondingly shortening the proton transfer pathway. The proton conductivities for the La and Pr complexes were roughly an order of magnitude higher than other members of the series (10^{-3} Scm^{-1} versus 10^{-4} Scm^{-1}). Single crystal structures of the high and low conducting members of the series (La, Pr for high and Ce for low) affirm the structural similarities extend beyond the unit cell parameters to positions of free acid groups and included water molecules. Scanning electron microscopy reveals marked differences in particle size of the different members of the Ln series owing to lattice strain effects induced by changing the lanthanide. Notably, the high conducting La and Pr complexes have the largest particle sizes. This result contradicts any notion that degradation of the MOF at grain boundaries is enabling the observed conductivity as proton conduction dominated by extrinsic pathways would be enabled by small particles (i.e. the La and Pr complexes would be the worst conductors). Proton conductivity measurements of a ball milled sample of the La complex corroborate this result.

Introduction

Better proton conducting membranes offer multiple benefits towards making hydrogen fuel cells more efficient. Development of new candidate proton conducting solids span many classes of compounds from macromolecular organic polymers to inorganic solid acids.[1] To design improvements to any material requires an ability to make a systematic change and assess the outcome of that change. Metal-organic frameworks (MOFs),[2] composed of metal ions or clusters connected via organic ligands to form multidimensional networks, are relatively recent candidates for proton conductors.[4-7] They are crystalline materials with modular synthetic pathways and contain pores, which could be loaded with various proton carriers – each of these offer opportunities for molecular based design and improved performance. In terms of proton conducting MOFs, given that a long-term target application would be in a steam-like environment in a fuel cell, water stability is critical for ultimate application and many water-stable MOFs have been identified. [8-11] That said, less stable materials can still provide molecular insights to conduction pathways and assist in the design of target structures provided ionic conductivity data reflects the molecular pathways.[12]

In any non-monolithic ion conductor, the conduction pathway spans both the bulk material and the interstices between particles, the grain boundary, creating both intrinsic and extrinsic conduction pathways. In systems such as ceramic oxide ion conductors, the physical and chemical difference between the bulk and grain boundary is typically significant resulting in the resolution of the two semicircular components in impedance spectroscopic analyses. Since the bulk proton conduction pathways in solids such as MOFs are hydrated micropores, the pathway would not be expected to vary to the same extent between the bulk and grain boundary. Indeed, clear resolution of the two impedance components for bulk and grain boundary contributions rarely occurs in the study of proton conducting MOFs under hydrated conditions. If the water stability of the MOF is questioned, this distinction becomes even more blurred and one could raise doubts about correlations between structure and activity in MOFs.[13] That said, the grain boundary is also a function of the material and a stable grain boundary is a necessary conduction pathway. However, a key question is whether measured ion conductivity arises despite the grain boundary or because of it.

Phosphonate groups are an intriguing functionality for proton conducting MOFs as they typically offer high water stability but also the potential for ligating as a hydrogen phosphonate giving more acidic pores.[5,7] We have previously reported the structure, $[La(H_5L)(H_2O)_4]$, La-PCMOF-5.[7] La-PCMOF-5 has, as notable features, high water stability, a well resolved proton conduction pathway including crystallographically

ordered free acid groups and water molecules, and an exceptionally low activation energy for proton transfer (0.17 eV) similar to solid acids. Given the well-visualized proton conduction network, La-PCMOF-5 offered an opportunity to develop a detailed structure-activity relationship if a means could be found to systematically vary the proton transfer pathway. As La-PCMOF-5 was synthesized using La^{3+} ions, it was hypothesized that replacing La^{3+} with smaller lanthanide ions would maintain the structure of the parent framework but contract the unit cell slightly. Thus, employing the lanthanide contraction should yield a series of isomorphous solids that would allow for fine tuning of the proton conduction pathway. Here, we report six lanthanide frameworks based on Ce^{3+}, Pr^{3+}, Nd^{3+}, Sm^{3+}, Eu^{3+} and Gd^{3+} which are isomorphous with La-PCMOF-5, the family henceforth denoted Ln-PCMOF-5. We report the synthesis, X-ray diffraction analyses, and proton conductivity of the Ln-PCMOF-5 family as well as new single crystal structures of the Pr^{3+} and Ce^{3+} complexes, two isomorphous compounds that differ by more than an order of magnitude in their proton conduction. The proton conduction measurements are assessed based on intrinsic and extrinsic conduction pathways and confirm that extrinsic degradation pathways are not part of the observed conductivity mechanism in this MOF family.

Experimental details

All reagents were purchased from commercial suppliers and used without further purification. A general synthetic procedure for $[Pr(H_5L)(H_2O)_4]$ (Pr-PCMOF-5) is included here as representative of the Ln-PCMOF-5 series. Further details on synthesis of H_8L and remaining Ln-PCMOF-5 structures along with experimental procedures are in the Supporting Information. Analogous preparations with Tb-Yb gave two different microcrystalline phases that were found to be non-proton conducting and were not studied in detail.

Synthesis of $[Pr(H_5L)(H_2O)_{4.4}]$ (Pr-PCMOF-5) and $[Ce(H_5L)(H_2O)_4]$ (Ce-PCMOF-5)

$Pr_2(CO_3)_3{\cdot}nH_2O$ (255 mg, 0.55 mmol) was combined with a 0.9M H_2SO_4 solution (3.3 mL, 2.97 mmol) and H_8L (251 mg, 0.55 mmol). After 24 hours, the solution yielded light green, crystalline particles (171 mg, 0.26 mmol, 47%). Elemental analysis calculated (%) for $PrC_{10}P_4O_{12}H_{15}{\cdot}4.4H_2O$: theoretical C 17.89, H 3.57; found: C 17.97, H 3.60. Thermogravimetric analysis, mass loss for water to 175˚C: Theoretical: 11.81%, Actual: 11.73%. Ln-PCMOFs were further characterized by powder X-ray diffraction, thermogravimetric and AC impedance analyses. To obtain crystals of Pr-PCMOF-5, a solution of $Pr(HSO_4)_3$ (0.1M, 10 mL) was prepared and added in 1mL portions to a vial containing crystals of La-PCMOF-5 (~300 mg) over several weeks until completely transferred. After 1 month, the block-shaped crystals slowly converted to needle-like crystals (Figure S15), one of which was then selected for X-ray structure refinement. Crystals of Ce-PCMOF-5 were synthesized in a similar manner as Pr-PCMOF-5. To crystals of La-PCMOF-5 was added a solution of $Ce(HSO_4)_3$ (0.1M, 10 mL). After several weeks, the block-like crystals of La-PCMOF-5 were converted to small, needle-like crystals. These crystals were too small for collection in-house; data was collected (at 100K) using synchrotron radiation (Si double crystal monochromator, Rayonix CCD detector and MD2 microdiffractometer) at the Canadian Light Source. Structure refinement and data solution details are provided in the ESI. The CIF files for Pr-PCMOF-5 (CCDC 1470115) and Ce-PCMOF-5 (CCDC 1499060) were deposited in the Cambridge Crystallographic Database.

Powder X-ray diffraction (PXRD) and Le Bail analysis

PXRD was performed on a Rigaku Miniflex II diffractometer in both continuous and step-mode; further details are included in the Supplementary Information. Use of the continuous scan mode for phase identification (2˚min-1, 0.02˚ scan width between 3-60˚ 2θ) revealed the structures of the six Ln-PCMOF-5 structures synthesized with Ce, Pr, Nd, Sm, Eu and Gd to be isomorphous to that of the parent La structure (Fig. S4, Supporting Information). Bragg-Bretano (θ, 2θ) XRD patterns were collected using a step-scan method (0.005˚, 6 sec per step), and refined against the simulated La-PCMOF-5 pattern using the Le Bail method.[14] The MAUD freeware package was used for the refinement.[15] Refinements were carried out successively on the scale factors, backgrounds and the cell parameters. Lattice parameters were retrieved for each of the compounds, and the final XRD patterns with the fits are shown in Figure S4.

Proton Conductivity Measurements

To determine the effect of the subtle structural changes on proton conductivity, AC electrochemical impedance measurements were performed on a Princeton Applied Research VersaSTAT3 potentiostat with environment maintained by an E-Spec BTL-433 humidity-controlled oven. Experiments were performed in air, at temperatures between 25˚C and 85˚C while humidity levels were maintained at 95% relative humidity (RH). Samples were finely ground to a powder by mortar and pestle prior to loading in custom dual-sample 2-probe cells with titanium electrodes. Electrodes were then tightened to 0.5 Nm using a torque screwdriver (rated between 0.1 to 1.2Nm) to ensure good contact. Cell (sample) lengths were approximately 1 mm with a 3.175 mm diameter, measured using calipers. As noted previously with La-PCMOF-5 the narrow 1-D channel sizes restrict fast equilibration of samples therefore at minimum three full heating/cooling cycles were performed with a minimum of 24 hours between temperature points. Duplicate measurements were obtained sweeping from 1MHz to 0.1Hz and then the same range in reverse. Data was collected using VersaStudio software (version 2.5).

Scanning Electron Microscopy/Energy Dispersive X-ray spectroscopy (SEM/EDX)

Samples were adhered to carbon tape on an Al pin and analyzed on a Zeiss SIGMA VP Field Emission SEM with backscatter electron detector. Chamber pressure was maintained at $1x10^{-7}$ bar, and an accelerating voltage of 2 keV was utilized from the thermal field emission source. EDX was collected at 20keV using an Oxford Instruments x-act system using a $10mm^2$ silicon drift detector. 2-D elemental maps were obtained to compare distribution of Ce, Pr and La along with phosphorus. All data collected was processed with INCA analysis software. After impedance measurements, samples were analyzed at the Instrumentation Facility for Analytical Electron Microscopy (IFFAEM) in the Dept. of Geosciences at the University of Calgary. Sample preparation was as above. An FEI Quanta 250 field emission gun (FEG) Samples were imaged with an accelerating voltage of 5keV under 50Pa vacuum.

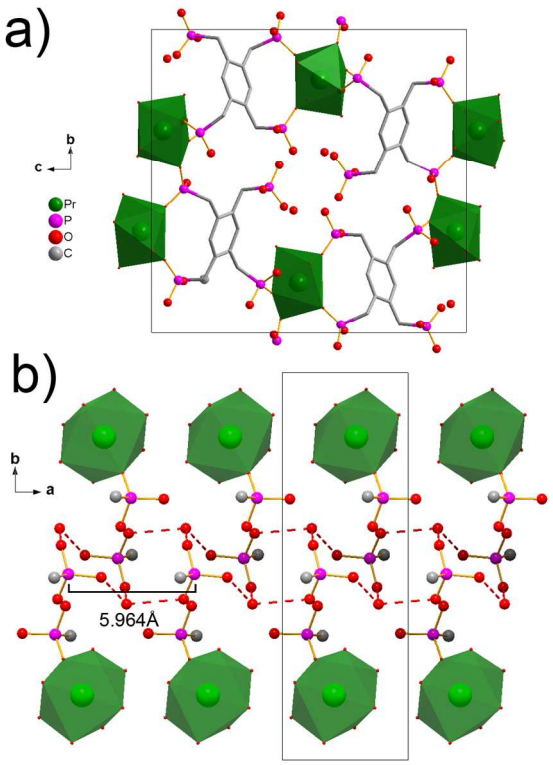

Figure 1. View of the crystal structure of Pr-PCMOF-5 along the **a)** a-axis with the free hydrogen phosphonates and **b)** along the c-axis showing the 1-D channel. The unit cell is also denoted along with unit cell a-length (also the P···P distance between adjacent hydrogen phosphonates).

Ball milling of La-PCMOF-5

A sample of La-PCMOF-5 was prepared as reported and placed in a Fritsch Pulverisette 6 planetary ball mill. Grinding took place at 200 rpm with zirconia beads in a 9:1 isopropanol:water solution. A subsample was obtained after 5 minutes which was filtered under vacuum, and air dried before AC impedance analysis at 95% RH.

Results and Discussion

The results of this study are presented largely chronologically as the experiments occurred as this delineation offers more insight into the experimental designs. Complexation of the lanthanides from La to Yb with H_8L gave three different phases of product. From Ce to Gd, the series of six lanthanides are isomorphous to La-PCMOF5. From Tb to Dy, a second phase is observed and from Er to Yb, a third phase is observed. These additional phases were determined not to be proton conducting and they also were found to have a different composition with a 7:6 M:L ratio (see ESI, Figs. S31, S32).

In the previous report by Taylor et al., La-PCMOF-5 was synthesized with La^{3+} through means of an acid modulator (H_2SO_4),[7] not unlike the use of HF in M(IV) phosphonate/phosphate systems.[16] While the addition of sulfuric acid also introduces the possibility of the metal sulfate as a competing product, lanthanide ions were chosen as they form water soluble hydrogensulfate salts. The use of acid thus played a dual role: 1) it inhibited the rapid precipitation of the metal phosphonate structure allowing the structure to order and give single crystals rather than an amorphous solid; 2) it made a more acidic solution giving free acidic groups in the product. This preparation method gave bulk powders of the isomorphous Ln-PCMOF-5 series but did not yield single crystals. PXRD, elemental analysis and thermogravimetry on bulk powders was performed to determine the phase purity and hydration state of the Ln-PCMOF-5 series.

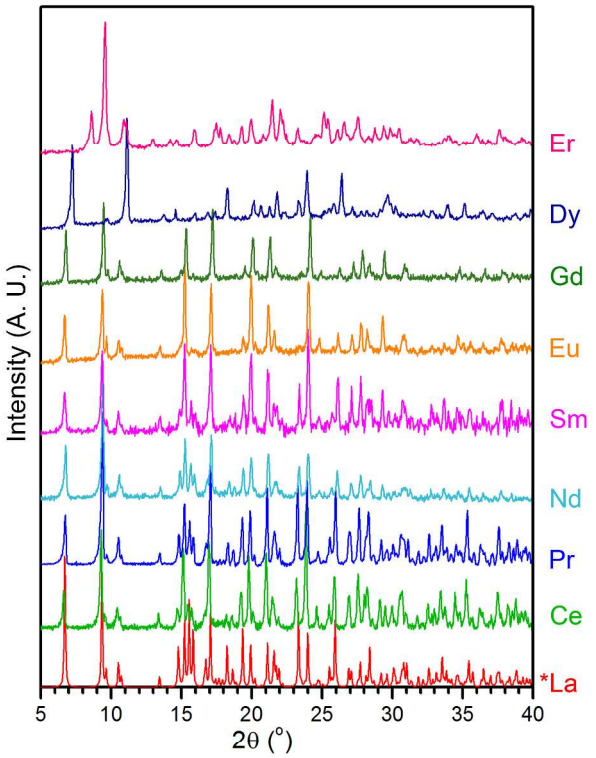

Figure 2. PXRD patterns of Ln-PCMOF-5: La to Gd, Dy, Er to show the isomorphous series up to Gd. Dy and Er show two other non-conducting phases.

Figure 1 shows the single crystals obtained for Pr-PCMOF-5. It is isomorphous to the original La-PCMOF5 and a brief description is provided. Pr-PCMOF5 has a 3-D structure where columns of phosphonate-bridged Pr ions are linked in two dimensions by H_5L^{3-} ions along the *a*-axis. The ligand utilizes three of the four phosphonate groups for coordination.

The uncoordinated group in Pr-PCMOF-5 is a hydrogen phosphonate (based on P···O bond distances of 1.503, 1.524 and 1.571Å, Figure S19). Of the three coordinating groups present in Pr-PCMOF-5, two are hydrogen phosphonates (P1, P3) while the final one is a phosphonic acid (P2). P···O distances in the phosphonic acid (about P2) were measured to be 1.485 Å, 1.537 Å, 1.557Å. In the hydrogen phosphonates, P···O distances were 1.519 Å, 1.521 Å, 1.571 Å about P1 and 1.502 Å, 1.512 Å, 1.580 Å about P3. In these two phosphonates, the shorter P···O distances belonged to the deprotonated O and double-bonded O (similar lengths due to delocalization of charge) while the longer bond is to the remaining OH. In Pr-PCMOF-5, the free hydrogen phosphonates (P4) or the coordinated phosphonic acids (P2) are located 6.000 Å away from the next respective, subsequent group along the a-axis of the unit cell, coinciding with the unit cell length. Water molecules located within the channel form an extensive hydrogen-bonded network with the phosphonic acids and hydrogen phosphonates.

Powder X-ray diffraction of the Ln-PCMOF-5 family, Ce to Gd, (Figure 2, S4) revealed solids isomorphous to La-PCMOF-5 for which single crystal data was previously reported. Eventually, the smaller Ln radii lead to two different phases for the six remaining Ln ions represented by the Dy and Er complexes. Refined unit cell parameters were extracted from Le Bail analysis of powder data at 298K for the Ln-PCMOF-5 family. All members of the Ln-PCMOF-5 family adopt $P2_1/c$ symmetry and show related unit cell parameters as well as the expected lanthanide contraction effect (Table 1). In La-PCMOF-5, the length of the *a*-axis corresponds to the distance between P atoms in adjacent hydrogen phosphonate groups along one wall of the 1-D channels (Figure 1b). Table 1 shows a systematic decrease in the length of the *a*-axis with the lanthanide contraction as expected with Ln cation radius obtained from Jia et al (Figure S14).[17] From the La to Gd structures, this distance decreases from 6.03 to 5.86 Å and this would be expected to impart a difference in the proton conduction properties.

Table 1. Unit cell parameters and R-factor obtained from LeBail fits of the Ln-PCMOF-5 series at 298K.

Ln	Ln^{3+} radii (Å)[17]	*a* (Å)	*b* (Å)	*c* (Å)	β (˚)	Vol (Å^3)	R (%)
La	1.15	6.031	18.347	19.040	95.541	2096.6	2.98
Ce	1.13	6.013	18.349	18.955	95.446	2085.5	2.98
Pr	1.11	6.000	18.356	18.966	95.505	2079.4	2.41
Nd	1.10	5.982	18.342	18.966	95.418	2072.0	2.53
Sm	1.08	5.970	18.347	18.979	95.572	2069.1	1.74
Eu	1.07	5.949	18.316	18.950	95.569	2055.3	2.03
Gd	1.05	5.855	18.080	18.684	95.272	1969.7	2.23

Thermogravimetric analysis of the as-prepared Ln-PCMOF-5 series revealed similarities, including a three-step mass loss (Figure S1). A large step, generally between 50˚C to 170˚C, corresponded to loss of coordinated and pore water. Two smaller, gradual mass losses typically from 170˚C to 325˚C and >325˚C are likely from condensation of the free phosphonic acid groups (pyrophosphate formation) and the onset of framework decomposition. La-PCMOF-5 has four water molecules per formula unit (three coordinated, one free). The Ln-PCMOF-5 series were hydrated (moles water/mole MOF) as 4.0 for Ce, 4.4 for Pr, 4.8 for Nd, 4.8 for Sm, 4.4 for Eu and 4.3 for Gd.

To characterize the proton conductivity, AC impedance measurements were performed on samples of Ln-PCMOF-5 at 95% relative humidity (RH) in air (Figure 3). Equilibration of these samples required several heating/cooling cycles to obtain consistent data owing to diffusional constraints in the micropores. Nyquist plots obtained for Ln-PCMOF-5 consisted of a single semicircle representative of both bulk and grain boundary resistances and a capacitive tail at the lower frequency region (towards 0.1 Hz) for the blocking effect of the titanium electrodes, an indication of ionic conductivity within the sample (Figure S5-S10). Proton conductivity values for the series at 85 ˚C and 95% RH are listed in Table 2. R^2 values for the slopes were obtained from a line of best fit of the plotted data and corresponding activation energies for each framework was calculated and included therein. Low E_{act} values are observed for the entire series and corroborate a Grotthuss mechanism as expected given the adjacent acid sites and free pore water. PXRD analysis after impedance revealed the powders maintained the same structures with slight peak broadening (Figure S3).

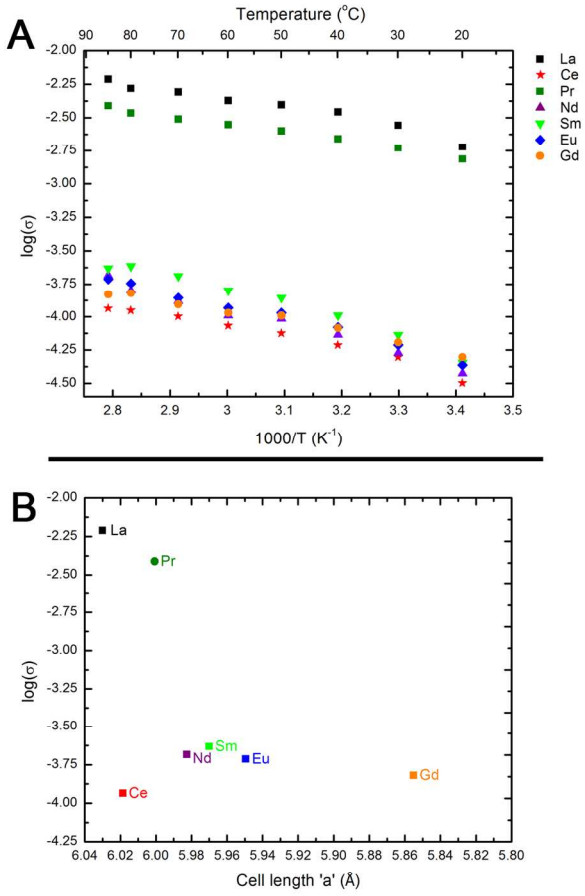

Figure 3. **A.** Conductivity vs. temperature plot for Ln-PCMOF-5 and **B.** Conductivity of Ln-PCMOF-5 vs. *a* axis length determined by LeBail analysis (Ln = La – Gd).

Table 2. Proton conductivities of the Ln-PCMOF-5 series at 85˚C, 95% RH with activation energies (E_{act}) and corresponding R^2 of Arrhenius plot.

Ln^{3+}	σ (Scm^{-1})	E_{act} (eV)	R^2 (best fit)
La	$6.0x10^{-3}$	0.17	0.96
Ce	$1.2x10^{-4}$	0.20	0.97
Pr	$3.9x10^{-3}$	0.17	0.99
Nd	$2.1x10^{-4}$	0.24	0.99
Sm	$2.3x10^{-4}$	0.24	0.96
Eu	$1.9x10^{-4}$	0.23	0.99
Gd	$1.5x10^{-4}$	0.19	0.98

There should be an optimum proton transfer distance between any proton donor-acceptor pair for efficient conduction of H^+ ions. Unit cell parameters (Figure S11-S13) and cell volumes were obtained from the LeBail refinements and plotted against conductivity at 85 ˚C, 95% RH (Figure 3B). The proton conductivity data for the Ln-PCMOF-5 family reveal that the La and Pr salts (3.9 - 6.0 $x10^{-3}$ Scm^{-1}) demonstrate more than an order of magnitude higher proton conduction than any other members of the series (1 – $2x10^{-4}$ Scm^{-1}). Based on the unit cell parameters, there is no anomalous change in structure as both the cell volume and the *a*-axis show a consistent decrease consistent with the lanthanide contraction (Figure S11). This dramatic difference in proton conductivity with apparent changes of <0.02 Å in inter-phosphonic acid group distances was surprising and the measurements on the higher conducting samples were reproduced on new samples. In the single crystal structures of La/Pr-PCMOF-5, free water molecules hydrogen bond between the hydrogen phosphonate and phosphonic acid groups and these are a part of the proton transfer pathway. The bulk solids did also show small differences in hydration between Ln-PCMOF-5 members but, from the TGA data, no direct correlation could be found between the water content of the Ln-PCMOF and conductivity (Figure S1-S2). Furthermore, the hydrolysis constants (i.e. $Ln^{3+} + H_2O \rightarrow Ln(OH)^{2+} + H^+$) of the lanthanides were also examined. Acidity decreases with atomic number hence the smaller ions are often more acidic. The lanthanides follow this trend and have similar values for $pK_{hydrolysis}$ = 8.5 for La, 8.3 for Ce, 8.1 for Pr[17] thus not explaining the high values in conductivity observed for La and Pr. It was hypothesized that the water positions within the structure greatly affected the conductivity beyond the contraction, so single crystals of Ce-PCMOF-5 were synthesized.

Based on recent work on single crystal transmetallation by Grancha et al.,[18] crystals of Pr-PCMOF-5 were obtained by a recrystallization process seeded by La-PCMOF-5 (see ESI). Large single crystals of La-PCMOF-5 were suspended in a 0.1 M solution of $Pr(HSO_4)_3$ for four weeks, wherein block-like crystals transformed into smaller, needle-like crystals (Figure S15) suitable for X-ray crystallography. Complete exchange of La for Pr was confirmed by SEM-EDX mapping (Figure S16, S17). Crystals of Ce-PCMOF-5 were grown in a similar manner, using a 0.1M solution of $Ce(HSO_4)_3$ solution. A subsample of the crystals was removed after 2 weeks for SEM/EDX mapping. The needle-like crystals, after 4 weeks, were analyzed crystallographically using synchrotron radiation. An overlay of the three structures of La,Pr,Ce-PCMOF-5 show very close correlation in atomic positions (Figure 4) in the three different Ln salts and confirms that the three structures are indeed very similar. In Figure 4, the positions of the metal atoms on the right side of the figure are superimposed and the structure grown to the left. The P···P distances belonging to the free phosphonates in La-PCMOF-5 are 5.5805(04) Å and 5.7995(40) Å viewed down the *a*-axis. The same P···P distances in Pr-PCMOF-5 are 5.5873(35) Å and 5.7670(35) Å and 5.5850(24) and 5.7773(25) Å in Ce-PCMOF-5. The hydrogen bonding distances between hydrogen phosphonate oxygens and the free water molecule are also similar. These distances are: in La-PCMOF-5, 2.6006(110) Å (O10···O5W) and 2.7514(109) Å (O11···O5W); in Ce-PCMOF-5, 2.6075(56) Å (O10···O1W) and 2.7228(58) Å (O12···O1W); in Pr-PCMOF-5, 2.6067(87) Å (O10-O16) and 2.7204(83) Å (O12···O16). The relevant hydrogen bonding distances which make up the network in the 1-D channels of La-PCMOF-5, Pr-PCMOF-5 and Ce-PCMOF-5 do not provide an obvious explanation into the observed differences in proton conductivities.

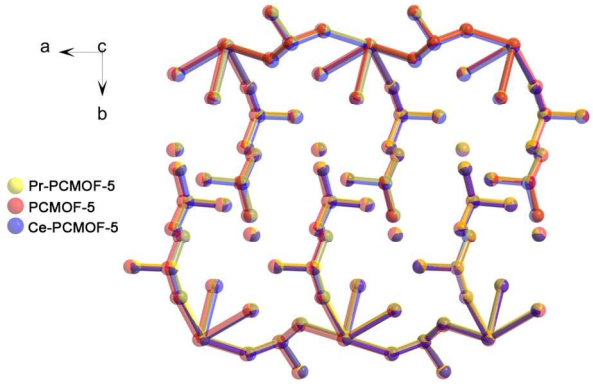

Figure 4. An overlay of the crystal structures of La-PCMOF-5, Pr-PCMOF-5 and Ce-PCMOF-5 to show similarities in atomic positions. The atoms on the left side of the image are superimposed and the structure permitted to vary to the right.

Given the similarity in the molecular structures of the Ln-PCMOF-5 series and, as mentioned, that in proton conducting MOF systems, impedance spectroscopy typically does not resolve bulk and grain boundary contributions. Scanning electron microscopy was carried out on all members of the Ln-PCMOF-5 series after impedance analysis. Horike et al. have discussed the opportunities availed to proton conducting coordination polymer systems through their many aspects of tunability including morphology.[3a] Ono et al. have also reported on grain boundary free conduction in MOF films.[19] Generally, in a good ion conductor, the grain boundaries are hurdles to performance rather than enablers of it as they disrupt the intrinsic conduction pathway. A full understanding of the role of a grain boundary is complex though as it is not just a function of the material but also a function of the given preparation as is well established in metal oxide ion conduction.[20]

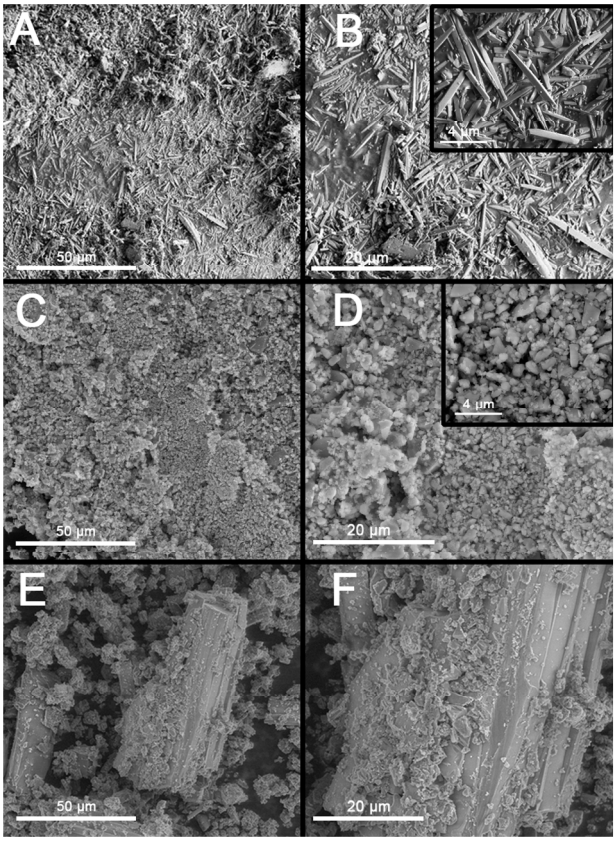

Figure 5. SEM images of La-PCMOF-5 (A, B), Ce-PCMOF-5 (C, D) and Pr-PCMOF-5 (E, F) after impedance measurements were completed. Scale bars at 50 µm and 20 µm for comparison show differences in particle size.

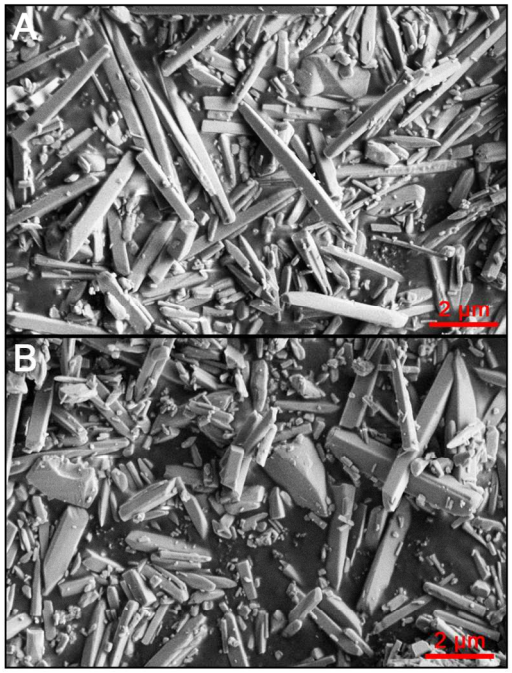

Figure 6. SEM images of A) pristine La-PCMOF-5 and B) after ball milling (5 min). 2µm scale bars are denoted.

Table 3. Mean particle sizes of Ln-PCMOF-5.

Ln-PCMOF-5	Avg particle size (µm)
La	1.71*
Ce	0.688
Pr	14.8
Nd	1.17
Sm	1.69
Eu	1.29
Gd	2.15

*NB. This value is underestimated due to the rod-like morphology of La-PCMOF-5.

SEM images of the post impedance samples (Figures 5, S21-S26) reveal significant differences in the particle size and morphology. In La-PCMOF-5, prepared for this study, the largest needle-like particles appear at ~10 µm in length while smaller sized particles ≤4µm are also present (Figure 5B, inset). In Ce-PCMOF-5, the particle sizes appear within a much narrower range and more uniform; estimated sizes are between 0.25 to 3 µm. In contrast however, Pr-PCMOF-5 has a wider variation in particle sizes: larger crystallites appear at around 50 µm with most particles at ~5 µm (Figure 5E, 5F). The largest particles appear to be intact crystals despite the treatment of the sample after impedance. Good interparticle contact within the pellet from the well aligned crystallites of Pr-PCMOF-5 would minimize grain boundary resistance and the overall alignment would be beneficial in maintaining proton hopping pathways. ImageJ was used to provide a particle size distribution from the SEM images (Figure S27, S28). Measurements were made on at minimum 300 particles to ensure good sampling with some caveats: only particles that were visible (not covered, buried, etc.) could be measured and particles >0.2µm were due to optical limitations. The mean particle sizes, calculated from the distributions obtained are shown in Table 3. These values do not capture the morphologies and aspect ratios of the different samples. La-PCMOF-5 has a needle-like morphology whereas Pr-PCMOF-5 is more plate-like. Ce-PCMOF-5 is much smaller and symmetrical. Thus, size differentials alone do not capture the full picture regarding possible differences in the grain boundary conductivities of these samples as the different morphologies will pack with different efficiencies regarding a conducting pathway. A facile 3-D diffusion pathway would be beneficial to proton conduction and spherical particles should promote that better than the rod-like particles observed for La-PCMOF5. However, this must be balanced with the packing efficiency of the individual interfaces and the efficiency of the extrinsic proton transfer pathway that results and this may be better in the case of rod-like particles.

To further study the effect of particle size on conductivity, pristine La-PCMOF-5 was ball milled for 5 minutes. SEM images obtained afterward showed an increasing number of smaller particles (<0.5 µm) with grinding time (Figure 6). PXRDs obtained after milling showed no difference in the pattern, indicating preservation of the structure in the particles (Figure S30). Particle sizing was again obtained using ImageJ and the average particle size determined (Figure S29). With increasing milling time, the average particle size does decrease and the distribution narrowed. In the pristine La-PCMOF-5

sample, the largest particles were found at 9.6 μm while the average size was 1.61 μm. After 5 minutes of milling, the largest particle was at 6.8 μm with an average size of 1.14 μm. The proton conductivity at 85°C and 95% RH for pristine La-PCMOF-5 was $6.0x10^{-3}$ Scm^{-1}. With 5 minutes of grinding, the conductivity fell to $1.3x10^{-4}$ Scm^{-1}. Thus, with the increasing milling time, and decreasing particle size, the conductivity dropped.

Table 4. La-PCMOF-5 Particle size with milling time

Time (min)	σ (Scm^{-1}) 85°C, 95% RH	Avg particle size (μm)
0	6.0×10^{-3}	1.71
5	1.3×10^{-4}	1.24

The Ln-PCMOF-5 series shows closely related structures at a molecular level. As expected, the substitution of successively smaller Ln ions forms an isomorphous series with gradual contraction of the unit cell. A coincident effect of changing the lanthanide ion is to impart a strain on the growing lattice and ultimately reduce the coordination number of the Ln ion. While the Ln-PCMOF-5 series from La to Gd is isomorphous, this lattice strain is evidenced by the vastly different particle sizes with each lanthanide. The radius change eventually leads to new phases with the smaller lanthanides, Tb -Dy form a second, non-conducting phase and Er-Yb form a third also non-conducting phase. It is germane that these latter phases are not proton conducting as, while not isomorphous to Ln-PCMOF-5, they are composed of the same phosphonate ligand and lanthanide ions. If degradation of the network at the particle interfaces was a determining factor in proton conduction, these second and third phases would also be expected to be proton conducting. Bazaga-García et al. reported an isomorphous series of eight lanthanide coordination polymers with nitrilotris (methylphosphonic acid).[21] Of the synthesized series, four were investigated (with La, Ce, Gd, Ho) where the proton conductivity spanned over 2 orders of magnitude. Su et al prepared an isostructural MOF series using imidazolium doped Fe, Ga, and Al phosphates.[22] Their proton conduction data also spans a factor of 40 between the three materials. In neither of the above works were grain boundaries evoked as a possible explanation. Taddei et al. have compared three Zr phosphonate MOFs and found that the smaller particle MOFs showed higher proton conduction although it must be emphasized that the MOFs were not isostructural.[23]

Tominaka and Cheetham have examined proton conduction in metal-organic frameworks and have suggested that extrinsic pathways can play a key or even dominant part of the high conductivities and low activation energies reported.[13] La-PCMOF-5 is a very low activation energy proton conductor, one of the lowest values reported for any MOF. In the Ln-PCMOF5 family, differences in particle morphologies and sizes are observed and these will unquestionably affect grain boundary conductivities. *However, if degradation/dissolution of the MOF at the particle surface was critical for the observed proton conductivity then the smaller particle samples would be expected to be much better proton conductors as they offer more interparticle surface to degrade regardless of morphology.* Indeed, all the small particle Ln-PCMOF members are the lower conductors (~10^{-4} Scm^{-1}) and La and Pr, which are more amenable to larger particles show the highest conductivities. This is corroborated by the conductivity of the pristine and ball-milled La-PCMOF-5 where the larger particle pristine sample showed better conductivity. That said, the present study does not establish the line between bulk and grain boundary conduction in this family. Indeed, between Ln-PCMOF-5 members, the differences in the extrinsic pathways appear greater than the intrinsic pathways and so the differences in conductivity appears to originate more in a stable grain boundary.

This outcome of this study as far as intrinsic and extrinsic proton conductivity in MOFs cannot be generalized to all MOF materials as each material will need to be assessed on its own stability and performance. Control of MOF morphology is an ongoing theme[24] for many applications as well as increased understanding of the role of defects in MOF properties including conduction.[25] *A highly conducting grain boundary is a positive feature of a material if it is a stable entity and permits reproducible ion conduction.* However, of course, it is desirable to apply molecular design to the features of a solid that would enable intrinsic conduction pathways. Finally, given the importance in metal-organic framework research placed on X-ray crystallography, in this work, crystal structures did not provide definitive answers to the observed conductivity. Rather, microcrystal size and morphology proved to be more insightful than the crystal structures themselves in understanding the differences in material properties.

Conclusions

We have reported a systematically altered series of proton conducting metal-organic frameworks, the Ln-PCMOF-5 family. Two members of this isomorphous family, La and Pr, demonstrated greater than an order of magnitude better proton conduction when single crystal structures showed that the molecular features of the series of solids were very highly correlated. Ultimately, large differences in particle size and morphology were observed between the low and high conducting members of the series with larger particle sizes observed for the two highest conducting members and smaller particles correlated with all the lower conducting members of the isomorphous series. The effect of the lanthanide contraction was two-fold in that: 1) the intrinsic molecular pathway was very finely altered and; 2) it resulted in dramatic differences in particle size, morphology and extrinsic conduction routes. The differences in conductivity are likely correlated to the difference in grain boundary but the conduction is not arising from degradation of the interparticle region as this would have made the smaller particle MOFs the better conductors.

ASSOCIATED CONTENT

Electronic Supplementary Information (ESI) available: Detailed experimental procedures, Le Bail fits, proton conduction data and full characterization of materials. See DOI: 10.1039/b000000x/

AUTHOR INFORMATION

Corresponding Author

Email: gshimizu@ucalgary.ca. Tel: +1 403 220 5347.

Author Contributions

The manuscript was written through contributions of all authors. All authors have given approval to the final version of the manuscript.

Funding Sources

We thank the Natural Sciences and Engineering Research Council (NSERC) of Canada for support of this research.

ACKNOWLEDGMENT

The authors acknowledge Dr. Hong-Cai Zhou for his suggestions on crystal growth and Dr. Chris DeBuhr at the Instrumentation Facility for Analytical Electron Microscopy (IFFAEM) at the University of Calgary, Department of Geosciences for assistance with the SEM samples.

ABBREVIATIONS

MAUD, Materials Analysis Using Diffraction; MOF; metal-organic framework; PCMOF, proton conducting metal-organic framework; PXRD, powder x-ray diffraction; RH, relative humidity; TGA, thermogravimetric analysis.

REFERENCES

(1) Haile, S. M.; Boysen, D. A.; Chisholm, C. R. I.; Merle, R. B., *Nature*, **2001**, *410*, 910–913.

(2) (a) Furukawa, H.; Cordova, K. E.; O'Keeffe, M.; Yaghi, O.M. *Science*, **2013**, *341*, 974-976. (b) Shekhah, O.; Liu, J. ; Fischer, R. A.; Woll, C.; *Chem. Soc. Rev*. **2011**, *40*,1081-1106, 2011. (c) Stock, N.; Biswas, S. *Chem. Rev*. **2012**, *112*, 933-969. (d) Cui, Y. J.; Li, B.; He, H. J.; Zhou, W.; Chen, B. L. ; Qian, G. D. *Acc. Chem. Res*. **2016**, *49*,483-493. (e) Bennett, T. D.; Cheetham, A. K. *Acc. Chem. Res*. **2014**, *47*, 1555-1562. (f) Morozan, A.; Jaouen, F. *Energy Env. Sci*. **2012,** *5*, 9269-9290. (g) Gagnon, K. J.; Perry, H. P. Clearfield, A. *Chem. Rev.*, **2012**, *112*, 1034–1054. (h) Li, S. L.; Xu, Q. *Energy Env. Sci.* **2013**, *6*, 1656-1683. (i) Zhu, Y.-P.; Ma, T.-Y.; Liu, Y.-L.; Ren, T.-Z.; Yuan, Z.-Y. *Inorg. Chem. Front.* **2014**, *1*, 360.

(3) (a) Horike, S.; Umeyama, D.; Kitagawa, S. *Acc. Chem. Res.* **2013**, *46,* 2376–2384. (b) Ramaswamy, P.; Wong, N. E.; Shimizu, G. K. H. *Chem. Soc. Rev.* **2014**, *43*, 5913–5932. (c) Yoon, M.; Suh, K.; Natarajan, S.; Kim, K. *Angew. Chemie Int. Ed.* **2013**, *52,* 2688–2700. (d) Yamada, T.; Otsubo, K.; Makiura, R.; Kitagawa, H. *Chem. Soc. Rev*. **2013**, *42*, 6655. (e) Li, . L.; Gao, Q.; Xu, J.; Bu, X. H. *Coord. Chem. Rev*. **2017**, *344*, 54-82.

(4)(a) Okawa, H.; Shigematsu, A.; Sadakiyo, M.; Miyagawa, T.; Yoneda, K.; Ohba, M.; Kitagawa, H. *J. Am. Chem. Soc.* **2009**, *131*, 13516-13522. (b) Hurd, J. A.; Vaidhyanathan, R.; Thangadurai, V.; Ratcliffe, C. I.; Moudrakovski, I. L.; Shimizu, G. K. H. *Nat. Chem.* **2009**, *1*, 705-710. (c) Bureekaew, S.; Horike, S.; Higuchi, M.; Mizuno, M.; Kawamura, T.; Tanaka, D.; Yanai, N.; Kitagawa, S. *Nat. Mater.* **2009**, *8*, 831-836.

(5) (a) Grohol, D.; Subramanian, M. A.; Poojary, D. M.; Clearfield, A. *Inorg. Chem.* **1996**, *35*, 5264–5271. (b) Taylor, J. M.; Mah, R. K.; Moudrakovski, I. L.; Ratcliffe, C. I.; Vaidhyanathan, R.; Shimizu, G. K. H. *J. Am. Chem. Soc.* **2010**, *132*, 14055-14057. (c) Colodrero, R. M. P.; Olivera-Pastor, P.; Losilla, E. R.; Aranda, M. A. G.; Leon-Reina, L.; Papadaki, M.; McKinlay, A. C.; Morris, R. E.; Demadis, K. D.; Cabeza, A. *Dalton Trans*. **2012**, 41, 4045. (d) Costantino, F.; Donnadio, A.; Casciola, M. Inorg. Chem. **2012**, *51*, 6992–7000. (e) Colodrero, R. M. P.; Olivera-Pastor, P.; Losilla, E. R.; Hernández-Alonso, D.; Aranda, M. A. G.; Leon-Reina, L.;Rius, J.; Demadis, K. D.; Moreau, B.; Villemin, D.; Palomino, M.; Rey, F.; Cabeza, A. *Inorg. Chem.* **2012***, 51*, 7689–7698. (f) Begum, S.; Wang, Z.; Donnadio, A.; Costantino, F.; Casciola, M.; Valiullin, R.; Chmelik, C.; Bertmer, M.; Kärger, J.; Haase, J.; Krautscheid, H. *Chem. Eur. J.* **2014**, *20*, 8862–8866. (g) Bao, S. S.; Otsubo, K.; Taylor, J. M.; Jiang, Z.; Zheng,L. M.; Kitagawa, H. *J. Am. Chem. Soc.* **2014**, *136*, 9292–9295 (h) Ramaswamy, P.; Wong, N. E.; Gelfand, B. S.; Shimizu, G. K. H. *J. Am. Chem. Soc.* **2015**, *137*, 7640-7643. (i) Pili, S.; Argent, S. P.; Morris, C. G.; Rought, P.; Garcia-Sakai, V.; Silverwood, I. P.; Easun, T. L.; Li, M.; Warren, M. R.; Murray, C. A.; Tang, C. C.; Yang, S. H.; Schroder, M. *J. Am. Chem. Soc.* **2016**, *138*, 6352-6355. (j) Kim, S.; Dawson, K. W.; Gelfand, B. S.; Taylor, J. M.; Shimizu, G. K. H. *J. Am. Chem. Soc.* **2013**, *135,* 963–966. (k) Bazaga-García, M.; Colodrero, R. M. P.; Papadaki, M.; Garczarek, P.; Zoń, J.; Olivera-Pastor, P.; Losilla, E. R.; León-Reina, L.; Aranda, M. A. G.; Choquesillo-Lazarte, D.; Demadis, K. D.; Cabeza, A. *J. Am. Chem. Soc*. **2014**, *136*, 5731–5739. (l) Bao, S. S.; Li, N. Z.; Taylor, J. M.; Shen, Y.; Kitagawa, H.; Zheng, L. M. *Chem. Mater*. **2015**, *27*, 8116-8125. (m) Cai, Z. S.; Bao, S. S.; Wang, X. Z.; Hu, Z.; L. M. *Inorg. Chem*. **2016**, *55*, 3706-3712. (n) Wei, Y. S.; Hu. X. P.; Han, Z.; Dong, X. Y.; Zang, S. Q.; Mak, T. C. W. *J. Am. Chem. Soc.,* **2017**, *139*, 3505–3512.

(6) (a) Horike, S.; Umeyama, D.; Inukai, M.; Itakura, T.; Kitagawa, S. *J. Am. Chem.Soc*. **2012**, *134*, 7612–7615. (b) Umeyama, D.; Horike, S.; Inukai, M.; Itakura, T.; Kitagawa, S. *J. Am. Chem. Soc*. **2012**, *134*,12780–12785. (c) Sen, S.; Nair, N. N.; Yamada, T.; Kitagawa, H. Bharadwaj, P. K.*, J. Am. Chem. Soc*., **2012**, *134*, 19432–19437. (d) Okawa, H.; Sadakiyo, M.; Yamada, T.; Maesato, M.; Ohba, M.; Kitagawa, H. *J. Am. Chem. Soc.* **2013**, *135*, 2256-2262. (e) Phang, W. J.; Lee, W. R.; Yoo, K.; Ryu, D. W.; Kim, B.; Hong, C. S. *Angew. Chem., Int. Ed*. **2014**, *53*, 8383-8387. (f) Nagarkar, S. S.; Unni, S. M.; Sharma, A.; Kurungot, S.; Ghosh, S. K. *Angew. Chem., Int. Ed*. **2014**, *53*, 2638-2642. (g) Nguyen, N. T. T.; Furukawa, H.; Gándara, F.; Trickett, C. A.; Jeong, H. M.; Cordova, K. E.; Yaghi, O. M. *J. Am. Chem. Soc*. **2015**, *137*, 15394-15397. (h) Aiyappa, H. B.; Saha, S.; Wadge, P.; Banerjee, R.; Kurungot, S. *Chem. Sci*. **2015**, *6*, 603-607. (i) Zhai, Q.-G.; Mao, C.; Zhao, X.; Lin, Q.; Bu, F.; Chen, X.; Bu, X.; Feng, P. *Angew. Chem., Int. Ed.* **2015**, *54*, 7886-7890. (j) Sadakiyo, M.; Yamada, T.; Kitagawa, H. *Chempluschem* **2016**, *81*, 691-701. (k) Zhang, F. M.; Dong, L. Z.; Qin, J. S.; Guan, W.; Liu, J.; Lu, M.; Lan, Y. Q.; Su, Z. M.; Zhou, H. C. *J. Am. Chem. Soc*. **2017**, *139*, 6183-6189. (l) Taylor, J. M.; Dekura, S.; Ikeda, R.; Kitagawa, H. *Chem. Mater*., **2015**, *27*, 2286–2289. (m) Inukai, M.; Horike, S.; Itakura, T.; Shinozaki, R.; Ogiwara, N.; Umeyama, D.; Nagarkar, S.; Nishiyama, Y.; Malon, M.; Hayashi, A.; Ohhara, T.; Kiyanagi, R.; Kitagawa, S. *J. Am. Chem. Soc.* **2016**, *138*, 8505-8511. (n) Chen, W. Q.; Horike, S.; Umeyama, D.; Ogiwara, N.; Itakura, T.; Tassel, C.; Goto, Y.; Kageyama, H.; Kitagawa, S. *Angew. Chem., Int. Ed.* **2016**, *55*, 5195-5200. (o) Nagarkar, S. S.; Horike, S.; Itakura, T.; Le Ouay, B.; Demessence, A.; Tsujimoto, M.; Kitagawa, S. *Angew. Chem., Int. Ed.* **2017**, *56*, 4976-4981. (p) Tominaka, S.; Coudert, F. X.; Dao, T. D.; Nagao, T.; Cheetham, A. K. *J. Am. Chem. Soc.* **2015**, *137*, 6428-6431. (q) Shalini, S.; Dhavale, V. M.; Eldho, K. M.; Kurungot, S.; Ajithkumar, T. G.; Vaidhyanathan, R. *Sci. Rep.* **2016**, *6*, 32489. (r) Li, R.; Wang, S. H.; Chen, X. X.; Lu, J.; Fu, Z. H.; Li, Y.; Xu, G.; Zheng, F. K.; Guo, G. C. *Chem. Mater*. **2017**, *29*, 2321-2331.

(7) Taylor, J. M.; Dawson, K. W.; Shimizu, G. K. H. *J. Am. Chem. Soc.,* **2013**, *135*, 1193–1196.

(8) (a) Schoenecker, P. M.; Carson, C. G.; Jasuja, H.; Flemming, C. J. J.; Walton, K. S. *Ind. Eng. Chem. Res.*, **2012**, *51*, 6513–6519. (b) Jasuja, H.; Burtch, N. C.; Huang, Y.; Cai, Y.; Walton, K. S. *Langmuir*, **2013**, *29*, 633–642.

(9) Duan, J.; Jin, W.; Kitagawa, S. *Coord. Chem. Rev*. **2017**, *332*,48-74.

(10) Gelfand, B. S.; Shimizu, G. K. H. *Dalton Trans.*, **2016**, *45*, 3668–3678.

(11) Howarth, A. J.; Liu, Y. Y.; Li, P.; Li, Z. Y. ; Wang, T. C. ; Hupp, J. T.; Farha, O. K. *Nat. Rev Mater*. **2016**, *1*, 15018.

(12) Joarder. B.; Lin, J. B.; Shimizu, G. K. H. *J. Am. Chem. Soc.,* **2017**, *139*, 7176-7179.

(13) Tominaka, S.; Cheetham, A. K. *RSC Adv.,* **2014**, *4*, 54382–54387.

(14) LeBail, A. *Powder Diffraction*. **2005**, *20*, 316.

(15) Lutterotti, L.;Bortolotti, M.; Ischia, G.; Lonardelli, I.; Wenk, H.-R. *Z. Kristallogr*., **2007**, *26*, 125-130.

(16) (a) Clearfield, A.; Wang, Z.; Bellinghausen, P. J. *Solid State Chem.,* **2002**, *167*, 376–385. (b) Alberti, G.; Casciola, M.; Costantino, U.; Peraio, A.; Montoneri, E. *Solid State Ionics,* **1992**, 50, 315–322.

(17) Jia, Y. Q. *J. Solid State Chem.,* **1991**, 95, 184–187.

(18) Grancha, T.; Ferrando-Soria, J.; Zhou, H.-C.; Gascon, J.; Seoane, B.; Pasán, J.; Fabelo, O.; Julve, M.; Pardo, E. *Angew. Chem. Int. Ed.,* **2015**, *54*, 6521–6525.

(19) Ono, K.; Ishizaki, M.; Kanaizuka, K.; Togashi, T.; Yamada, T.; Kitagawa, H.; Kurihara, M. *Angew. Chem. Int. Ed*. **2017**, *56*, 5531-5535.

(20) (a) Norby, T. *Mater. Res. Soc. Bull.* **2009**, *34*, 923-928. (b) Pergolesi, D.; Fabbri, E.; D'Epifanio, A.; Di Bartolomeo, E.; Tebano, A.; Sanna, S.; Licoccia, S.; Balestrino, G.; Traversa, E. *Nature Mater.* **2010**, *9*, 846-852. (c) Chen, C.-T.; Danel, C. E.; Kim, S. *J. Mater. Chem.* **2011**, *21*, 5435-5442. (d) Yamazaki, Y.; Hernandez-Sanchez, R.; Haile, S. M. *Chem. Mater*. **2009**, *21*, 2755-2762.

(21) Bazaga-García, M.; Angeli, G. K.; Papathanasiou, K. E.; Salcedo, I. R.; Olivera-Pastor, P.; Losilla, E. R.; Choquesillo-Lazarte, D.; Hix, G. B.; Cabeza, A.; Demadis, K. D. *Inorg. Chem.* **2016**, *55*, 7414-7424.

(22) Su, X. L.; Yao, Z. Z.; Ye, Y. X.; Zeng, H.; Xu, G.; Wu, L.; Ma, X. L.; Chen, Q. H.; Wang, L. H.; Zhang, Z. J.; Xiang, S. C. *Inorg. Chem.* **2016**, *55,* 983-986.

(23) Taddei, M.; Donnadio, A.; Costantino, F.; Vivani, R.; Casciola, M. *Inorg. Chem.* **2013***, 52*, 12131-12139.

(24) (a) Hirai, K.; Reboul, J.; Morone, N.; Heuser, J. E.; Furukawa, S.; Kitagawa, S. *J. Am. Chem.Soc*. **2014**, *136*, 14966-14973. (b) Umemura, A.; Diring, S.; Furukawa, S.; Uehara, H.; Tsuruoka, T.; Kitagawa, S. *J. Am. Chem.Soc*. **2011**, *133*,15506-15513.

(25) (a) Montoro, C.; Ocon, P.; Zamora, F.; Navarro, J. A. R. *Chem. Eur. J.* **2016**, *22*, 1646-1651. (b) Taylor, J. M.; Komatsu, T.; Dekura, S.; Otsubo, K.; Takata, M.; Kitagawa, H. *J. Am. Chem. Soc.* **2015**, *137*, 11498-11506. (c) Sholl, D. S.; Lively, R. P. *J. Phys. Chem. Lett.* **2015**, *6*, 3437-3444. (d) Fang, Z. L.; Bueken, B.; De Vos, D. E.; Fischer, R. A. *Angew. Chem. Int. Ed.,* **2015**, *54*, 7234-7254.

SYNOPSIS TOC: